Core-Shell Microgel-Based Surface Coatings with Linear Thermoresponse

Marian Cors, Oliver Wrede, Anne-Caroline Genix, Dario Anselmetti, Julian Oberdisse, Thomas Hellweg

Core-shell microgel based surface coatings with linear thermo-response

Marian Cors[1, 2], Oliver Wrede[1], Anne-Caroline Genix[2], Dario Anselmetti[3], Julian Oberdisse[2], Thomas Hellweg[1]

[1] *Department of Physical and Biophysical Chemistry, Bielefeld University, Universitaetsstr. 25, 33615 Bielefeld, Germany*

[2] *Laboratoire Charles Coulomb (L2C), CNRS, Université de Montpellier, 34095 Montpellier, France*

[3]*Department for Experimental Biophysics and Applied Nanoscience, Bielefeld University, Universitaetsstr. 25, 33615 Bielefeld, Germany*

Abstract

We study the swelling and shrinking behavior of core-shell microgels adsorbed on silicon wafers. In these systems, the core is made of cross-linked poly(*N*-isopropylmethacrylamide) and the shell consists of cross-linked poly(*N*-n-propylacrylamide). In suspension, these particles exhibit an extended linear swelling behavior in the temperature interval between the lower critical solution temperatures of the two polymers. Using ellipsometry and AFM, we show that this linear response is also observed in the adsorbed state.

Introduction

Acrylamide-based microgels are colloidal particles comprising a gel network of solvated polymer chains.[1] As a function of external stimuli, and in particular temperature, these particles show a reversible shrinking and swelling behavior granting them the name "smart microgels".[2–5] The most prominent examples are microgels based on poly(*N*-isopropylacrylamide) (pNIPAM)[6,7], which have a volume phase transition temperature of ca. 32–33 °C in water, corresponding to the lower critical solution temperature (LCST) in the phase diagram.[8] However, also other monomers lead to the formation of microgels with thermo-responsive behavior, with various phase transition temperatures.[9–14] By copolymerizing them statistically, the phase transition temperature can be tuned.[11,15–20] Moreover, by designing complex particle architectures[4,21–30], i.e. microgel particles with compartments of different monomeric composition or composition gradients, particle properties are expected to be varied, and stimuli-response controlled. Furthermore, also the properties of single adsorbed microgels and of microgel coatings have been studied.[31–39] A core-shell architecture, where the core and the shell have a different phase transition temperature is particularly promising. Zeiser et al. have recently shown that for core-shell particles with a shell of smaller LCST than the core, a *qualitatively* different bulk swelling behavior is present, including a linear swelling over a broad range of temperatures.[26]

Beside the scientific interest in this volume phase transition, growing attention arises from potential applications of these materials. Prominent examples are their use as surface coatings for smart cultivation of vertebrate cells and as etalons.[34,40–43] In this context, using different particle architectures might be advantageous, as it would allow making use of progressive swelling/shrinking as a function of temperature, as opposed to a sudden collapse. However, it remains to be shown that core-shell microgels made of poly(*N*-isopropylmethacrylamide) (pNIPMAM) and poly(*N*-*n*-propylacrylamide) (pNNPAM) still exhibit a linear swelling response in the adsorbed state. Hence, in this article, we focus on core-shell microgels made of a large pNIPMAM core having a high LCST of 44°C, surrounded by a shell of pNNPAM having an inferior LCST of 21°C, similar in architecture to those described by Zeiser et al[26]. The magnitude of the response of these core-shell microgels is mainly controlled by the cross-linker content of the core if the shell composition is chosen to be constant. Therefore, in this work we systematically vary the core crosslinker content (CCC) of the pNIPMAM cores. Both the swelling properties of the cores and of the core-shell microgel particles are studied in suspension by photon correlation spectroscopy (PCS) first. Then the particles are deposited on a silicon wafer by spin-coating, and the thickness of the layer and individual height profiles are studied by AFM and ellipsometry in the dry state, followed by an investigation of the swelling properties when the layers are covered with water.

Experimental Section

Synthesis: The core monomer *N*-isopropylmethacrylamide (NIPMAM, purity > 97 %), the initiator ammonium peroxodisulfate (APS, >98 %), the crosslinker *N*,*N*'-methylenebisacrylamide (BIS, 99 %), the ionic surfactant sodium dodecyl sulfate (SDS, >99 %) were purchased from Sigma-Aldrich and used as received. The shell monomer *N*-*n*-propylacrylamide was synthesized following a classical Schotten-Baumann reaction described by Hirano et al.[44], using acryloyl chloride (97 %, Aldrich, USA), triethylamine (99 %, Grüssing, Germany), propylamine (99 %, Fluka, USA) and methylene chloride (p. A.) as solvent. For the synthesis of pNIPMAM cores with different crosslinker contents, a 250 mL three-necked flask under gentle nitrogen flow with a mechanical stirrer on the top opening is used. This flask was placed in a heating oil bath with magnetic stirrer. The two side openings were equipped with a septum with a cannula as nitrogen inlet and a reflux condenser with bubble counter, respectively. The crosslinker contents, SDS concentration and radical starter specified as mol% with respect to the amount of monomer are listed in Table 1 for all samples. The crosslinker was dissolved in water (140 mL) first and subsequently heated to 70 °C. Its concentration in the core is given as CCC (core crosslinker content) throughout this article. After purging the solution for 1 h with nitrogen the monomer followed by surfactant was added as powder and after 5 minutes the reaction was initiated by injecting 1 mL of an aqueous solution of the radical starter. After rinsing the neck of the flask and initiation the volume was 150 mL. The total reaction took 5 h, followed by continued stirring at room temperature overnight, and purification. The purification was done at room temperature by centrifugation at 48,384 g for 45 minutes, decantation of the supernatant and redispersion of the precipitate with water. The redispersion was dome with a vortexer (MS 3 basic, IKA-Werke GmbH & CO. KG, Staufen, Germany) for typically 1 minute at maximum speed. This procedure was repeated five times. Shell synthesis was done with a similar protocol, also at high temperature and thus in the collapsed state, in the same setup with a 100 mL flask, by precipitating NNPAM on previously synthesized and purified pNIPMAM cores resulting in a pNIPMAM-core pNNPAM-shell microgel system. The total suspension volume was 50 mL. The shell had always the same nominal composition. The amount of crosslinker BIS was 1.90 mol% with respect to the NNPAM feed and the added amount of the core was 0.15 wt% with respect to the solvent. The concentration of SDS was 1.1 mmol per Liter (2.75 mol%). The core-shell particles were again purified by the same purification procedure as the core particles.

Table 1: pNIPMAM-core crosslinker (BIS) content. Constant amounts of pNIPMAM (12.4 mmol, 1.5628 g ± 0.0004 g), SDS (3 mol%, 1.0730 g ± 0.0010 g) and radical starter (3.3 mol%, 0.0924 g ± 0.0001 g) were used.

BIS / mol%	BIS / g
5.00	0.0947
7.50	0.1421

10.00	0.1894
12.50	0.2368
15.00	0.2841

The resulting molecular architecture is depicted in Scheme 1.

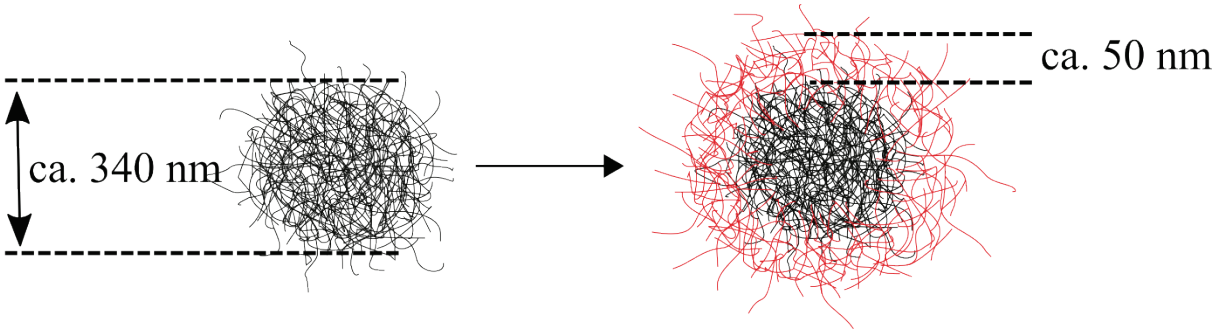

Scheme 1: Core-shell architecture obtained by precipitating and cross-linking of NNPAM (red) on the pNIPMAM core (black). The collapsed core particles are used as seeds in the precipitation polymerization of pNNPAM. The shell synthesis is done at 70 °C, which is largely above both LCSTs of the two polymers.

Photon correlation spectroscopy (PCS): PCS experiments were performed using two different setups. Angular dependent PCS experiments were done using a classical goniometer setup (ALV GmbH, Langen, Germany) equipped with an Ar^+-ion laser (Stabilite 2017, Spectra Physics, Santa Clara, USA) emitting at 514.5 nm. The sample was placed in a decalin matching bath kept at constant temperature using a thermostat (Haake DC50, Thermo Fisher Scientific, Waltham, USA). The scattered light was analyzed using a multiple τ hardware correlator (ALV 5000 Fast, ALV GmbH, Langen, Germany). The obtained correlation functions were analyzed using numerical Laplace inversion by means of CONTIN [45,46]. This method provides the intensity-weighted relaxation rate Γ of the observed dynamics in the sample. For pure diffusional modes the dispersion $\Gamma \sim q^2$ is expected and the diffusion coefficient can be obtained from the corresponding plot. The expected dispersion is found for both the core and for the core-shell particles. Hence, the temperature-dependent measurements were performed at a fixed angle of = 60 ° in a partly home-made setup. The PCS-setup had a He-Ne laser (HNL210L-EC, 632.8 nm, Thorlabs, Newton, USA) as light source, a multiple tau digital correlator (ALV-6010, ALV GmbH, Langen, Germany) and a detector (SO-SIPD, ALV GmbH, Langen, Germany). The sample was placed in a decalin matching bath. For temperature control a refrigerated bath (Haake C25P, Thermo Fisher Scientific, Waltham, USA) with a controller (Phoenix II, Thermo Fisher Scientific, Waltham, USA) was used.

Spin coating: Microgel monolayers on silicon wafers (Sigert Wafer, diameter = 50.8 mm, Aachen, Germany) were obtained by spin coating (LabSpin6, SÜSS micro Tec, Garching, Germany), after plasma cleaning (Zepto B, Diener Electronics, Ebhausen, Germany) with an O_2-plasma for 15 min at 100 W. The calculated arithmetical mean deviation roughness as well as the root mean square roughness was below 1nm. For microgel layers with a high surface coverage first, a dilute purified microgel dispersion (0.5 wt%) was put on the whole silicon wafer for 45 min, followed by spinning for 300 s at a rotation speed of 1000 rpm. For well-separated microgel particles the same procedure was used without waiting 45 min before spinning the wafer.

Ellipsometry: For ellipsometry measurements a single-wavelength ellipsometer (SE 400adv, SENTECH Instruments GmbH, Berlin, Germany) was used. The method of ellipsometry was described elsewhere.[47,48] Temperature control and liquid cell are custom-made products from SENTECH. The accessible temperature range was 15 °C to 55 °C. The measurements and modeling were done with the software "SE400advanced" from SENTECH. For modeling, a first guess of the microgel layer thickness was used based on the layer thickness determined by AFM measurements, and the initial refractive index was estimated based on literature to 1.35.[31] Ellipsometry was already used to characterize the swelling behavior of adsorbed microgels in our previous work from Schmidt et al.[31] and in literature.[49]

AFM: AFM measurements were performed on a FlexAFM (Nanosurf AG, Liestal, Switzerland) with an Easyscan 2 controller (Nanosurf AG, Liestal, Switzerland). To avoid background vibrations, the AFM was placed on a sample stage (Flex, Nanosurf AG) on top of a marble plate which lies on tennis balls. All measurements where performed in tapping ("Phase Contrast") mode. We used standard silicon cantilevers with 30 nm aluminum reflex coating from BudgetSensors® (Tap300Al-G, BudgetSensors®, Sofia, Bulgaria). The cantilevers had a force constant of 40 N/m and a resonance frequency of approximately 290 kHz. The scan rate was between 1 Hz and 0.33 Hz with 256 or 512 points per line. The setpoint was 55 % of the maximal deflection and the free vibration amplitude was approximately 200 mV.

The thickness of the dry microgel monolayer was determined as the average height over an area of 25 μm^2 using the software of the AFM (Nanosurf Easyscan 2, Nanosurf AG, Liestal, Swiss). For investigation of the individual height profiles of single microgels, we analyzed the recorded raw data with the open source data evaluation program for scanning probe microscopy Gwyddion.[50] After background correction we extracted the profile of at least 20 microgels and calculated the mean profile.

Determination of the amount of water of dried microgels: The water content of dried microgels can be determined by Karl-Fischer titration.[51] The measurements were done using a Karl-Fischer coulometer (684 KF Coulometer, Metrohm AG, Herisau, Swiss). The titration solution was CombiCoulomat fritless (Meck KGaA, Darmstadt, Germany). The microgels were dried for 24 h at 70 °C in a drying oven (U30, Memmert GmbH + Co. KG, Schwabach, W - Germany) and after storing them for 24 h at ambient they

were dissolved in methanol (Methanol AnalaR NORMAPUR® ACS, Reag. Ph. Eur. zur Analyse, VWR International, Radnor, USA) resulting in a solution of 1 wt%. The measurements was done with a sample volume of 100 µL. The water content of the solvent was measured and subtracted.

Results and Discussion

After microgel synthesis, the particles have been characterized in aqueous suspension first. Then they have been deposited on silicon wafers by spin-coating, and their swelling properties in the dry and wet state have been investigated by ellipsometry. Moreover, AFM has been used to measure the height profile of individual dry microgel particles.

Synthesis and properties in suspension

The microgel cores were produced following the synthesis protocol outlined in Section 2 and the parameters are summarized in Table 1. The key parameter is the core crosslinker content (CCC), which allows fine tuning of the global swelling properties of the core-shell particles in suspension.[26] We have first checked that the cores alone have the expected swelling properties of pNIPMAM, see Supporting Information Figure S1 for details. Then, we have measured the hydrodynamic radius R_H as a function of temperature of the series of core-shell microgels by PCS. These results are shown in Figure 1. They agree nicely with previous findings by Zeiser et al[26] and thereby validate the synthesis.

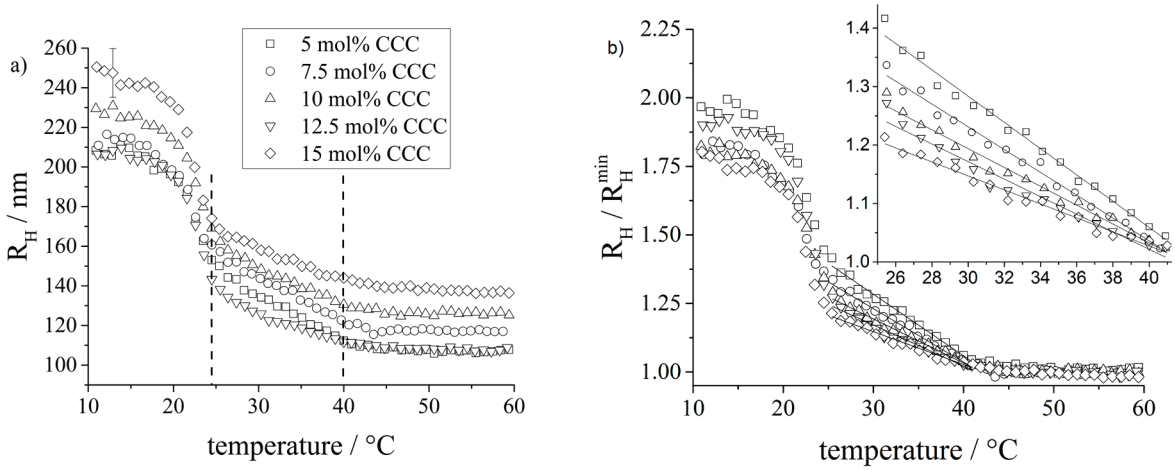

Figure 1: Swelling curves of core-shell microgels as a function of temperature with different core crosslinker contents (CCC) (5.0 mol% CCC (□), 7.5 mol% CCC (○), 10.0 mol% CCC (△), 12.5 mol% CCC (▽) and 15.0 mol% CCC (◇)). **a)** Hydrodynamic radius R_H. The linear swelling zone is indicated by the vertical dashes. An example of the error of PCS data estimated to be 5% is indicated. **b)** Same data normalized with respect to the high-temperature average (T = 45 C° – 50 °C) of the hydrodynamic radius R_H^{min}. Inset: Zoom of the linear region.

The original swelling curves shown in Figure 1a display the hydrodynamic radius R_H as a function of temperature, for microgel suspensions of various CCC as given in the legend. Three swelling regimes

are found. Below T = 20 °C, the entire particles are swollen, and the total hydrodynamic radius is typically greater than 200 nm. Note that due to the different formulations with the various crosslinker concentrations, the total swollen sizes of the core-shell microgels are not identical. At the VPTT of pNNPAM (23 °C), the system starts to collapse, resulting in a size transition step. The region of interest in the intermediate temperature range, between 23 °C and 44 °C, shows a swelling behavior where R_H changes *linearly* with temperature. Instead of some average transition temperature with a steep collapse, the swelling extends thus over the entire temperature range. At high temperature, finally, both core and shell are collapsed. A second size transition step at the VPTT of pNIPMAM (44 °C) does not occur because the particle size is already compressed to the range of the collapsed core (compare Figure S1). As the microgels do not have the same size from the start, it is instructive to normalize the size by the collapsed radius R_H^{min} taken as the high-temperature average (T = 45 – 50 °C). The result, R_H/R_H^{min}, is shown in Figure 1b, where the high temperature regime now superimposes by construction. This representation illustrates that the swelling is higher for the samples with lower CCC. The slope in the linear regime connecting the collapsed and the swollen state can therefore be tuned by the core crosslinker content.

A zoom of the linear region is given in the inset of Figure 1b for different crosslinker concentrations. The relative value of the slope is found to decrease from 2.25 %/°C to 1.22 %/°C, with reasonable accuracy (± 0.06 %). These values are in line with the total relative decrease of about 30 % in radius, over a temperature range of some 15 degrees. The change in slope corresponds to a diminished sensitivity of swelling to temperature by a factor of 1.8, when the CCC is changed from 5 to 15 mol%.

Finally, the swelling is sometimes expressed in terms of volume change which is given by $(R_H/R_H^{min})^3$. This leads to a qualitatively similar figure as Figure 1b, with the linear domain slightly curved, and the low-temperature values giving the maximum volumetric swelling. In our case, the maximum swelling varies from about six to eight with CCC.

Spin coating and characterization of dry surfaces

Well-separated core-shell microgel particles have been deposited by spin coating on silicon wafers, and studied by AFM. The height profiles of individual particles in the dry state can be determined by image treatment of the AFM results, and averaged over several particles, typically 20. In the SI (Figure S3), sample measurements are shown for illustration.

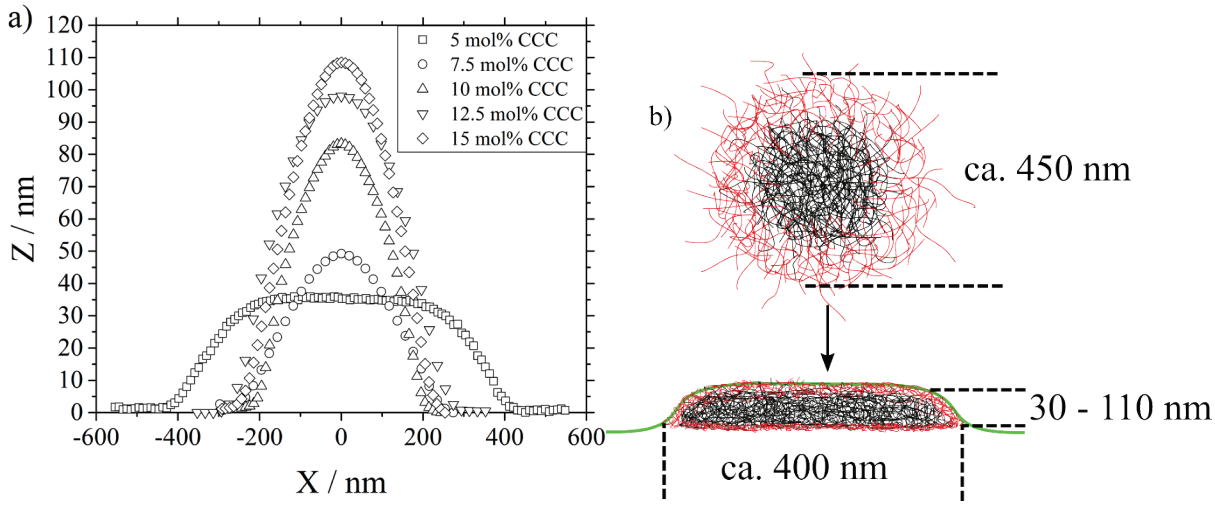

Figure 2: a) Average height profiles for dry core-shell microgels determined from AFM height scans, for different core crosslinker contents as indicated in the legend. b) Schematic drawing of a microgel in suspension and an adsorbed microgel.

In Figure 2a, the average height profiles for microgels with different CCC are shown. One should pay attention to the different X- and Z-scales: all microgel particles are squeezed and adopt a rather flat, pancake-like shape. With increasing CCC, the particles become less flat: an increase in CCC by a factor of three from 5 to 15 mol% results in an increase in height by a factor of three as well, but even particles with the highest degree of crosslinking have an aspect ratio of ca. four. Figure 2b shows a schematic drawing of an adsorbed microgel particle. The total volume of these pancakes can be determined by integration, i.e. adding up the volume of hollow cylinders delimited by the height profile. If this volume is taken as the microgel volume (with water) then the total polymer volume (without water) can be determined by subtraction of the volume of the water present in the "dry" sample, determined by Karl-Fischer-Titration. Then the water contents can be determined by comparing the polymer volume (without water) to the swollen (low-T) volume in water estimated from PCS. The calculated volumes are given in Table 2. From the ratio of the swollen to the dry volume, a water content of ca. 75-95 % in the swollen state can be deduced. This is approximately four times higher compared to the water content of dried microgels ($\Phi_{H2O,dry}$) of about 20 % residual water. The water content in the dried state was determined by Karl-Fischer-Titration.

Table 2: Volume of dry core-shell microgels estimated with the average height profiles determined by AFM (Figure 3), comparison to volumes in suspension (PCS), estimated water fractions in suspension, in the swollen state ($\Phi_{H2O,sw}$) and measured water contents in the dried state ($\Phi_{H2O,dry}$) by Karl-Fischer-Titration for different core crosslinker contents (CCC).

Core crosslinker content / mol%	$V_{dry.}$ / nm^3	$V_{collapsed}$ / nm^3	$V_{swollen}$ / nm^3	$\Phi_{H2O,dry}$	$\Phi_{H2O,\ sw}$
5	$1.19 \cdot 10^7$	$5.13 \cdot 10^6$	$3.88 \cdot 10^7$	18 %	74 %
7.5	$3.61 \cdot 10^6$	$6.71 \cdot 10^6$	$4.46 \cdot 10^7$	17 %	93 %
10	$4.84 \cdot 10^6$	$8.58 \cdot 10^6$	$5.44 \cdot 10^7$	22 %	93 %

12.5	$9.17 \cdot 10^6$	$5.42 \cdot 10^6$	$3.88 \cdot 10^7$	19 %	80 %
15	$7.66 \cdot 10^6$	$1.15 \cdot 10^7$	$6.95 \cdot 10^7$	22 %	91%

As a next step, successful deposition of microgel particles with a high surface coverage was obtained by spin coating on silicon wafers, following the protocol given in Section 2. The optimization of system parameters, and in particular the introduction of a waiting time of 45 minutes before spinning, as well as the appropriate concentration, were essential to promote the formation of homogeneous layers. In Figure 3, an AFM height profile scan over a lateral size of 5 µm of a dry microgel particle layer at room temperature (22±1 °C) is presented. It shows that the core-shell particles cover the surface, forming a dense monolayer. The mean height of an area of 25 μm^2 was determined and is given in Table 3. To verify homogeneity of the surface coating, different magnitudes up to an image with 50 µm lateral size are shown in the SI (Figure S2).

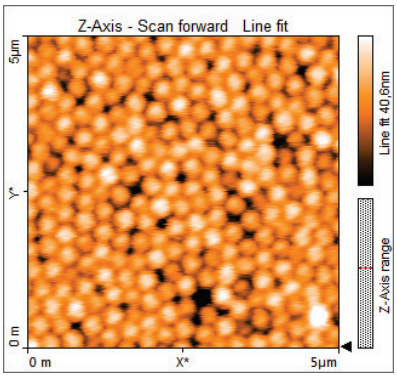

Figure 3: Zoom of an AFM height scan of a monolayer of dried core-shell microgels with 5 mol% core crosslinker content. The lateral image size is 5 µm and the average height is 30.8 nm.

Given that the geometry in Figure 3 is not a laterally homogeneous flat layer due to the density fluctuations caused by the array of squeezed spherical microgel particles and the presence of holes, the average thickness of the dry layers determined by AFM has been confirmed by ellipsometry. The ellipsometry measurements yielded also the refractive index of the microgel particles. Both thickness measurements are compared in Table 3.

Table 3: Thickness of dried layers of core-shell microgel particles deposited on a wafer, measured by AFM and ellipsometry. The thickness was deduced by the mean thickness of an area of 25 μm^2 for AFM and ca. 1 mm^2 for ellipsometry. The refractive index was determined by ellipsometry. The error of thicknesses determined by AFM is estimated to be 5 % based on multiple measurements.

Core crosslinker content (mol%)	Thickness AFM (nm)	Thickness by ellipsometry (nm)	Refractive index by ellipsometry
5	30.8	36.0±0.8	1.48±0.02
7.5	46.8	41.1±0.9	1.51±0.02
10	59.6	51.8±1.2	1.50±0.02
12.5	71.8	56.0±1.2	1.49±0.02
15	74.5	64.0±1.4	1.46±0.01

The general tendency of increase in thickness with CCC is well captured by both methods, and the results agree at least semi-quantitatively. The difference in thickness determined by AFM and ellipsometry may be due to surface roughness. While AFM measures the detailed topography of the microgel surface, and average height can be easily computed, single wavelength ellipsometry averages over the layer. Then surface roughness like the one due to the individual microgel particles contributes, and may result in an inaccuracy in thickness.[52]

Comparison of swelling in water at surfaces and in bulk suspension

The thicknesses in water of the core-shell microgel layers obtained by spin coating on silicon wafers have also been assessed with ellipsometry. The raw results are plotted as a function of temperature in Figure 4a, for three different CCC as given in the legend. At low temperature, the total thicknesses are a bit smaller than twice the hydrodynamic radii in suspension (cf. Figure 1a), which can be understood from the probable fuzzy nature of the particle surface, not dense enough to be picked up by ellipsometry. Moreover, particles are probably slightly deformed upon contact with the wafer. The ellipsometric thickness is found to be about 70% to 85% of the hydrodynamic diameter, which seems to be compatible with such a scenario. Furthermore, as the initial microgel particles differ in size due to the varying compositions, their thicknesses d is normalized to the unswollen, high-temperature (45 °C – 50 °C) thickness d^{min} in Figure 4b, in analogy to Figure 1b.

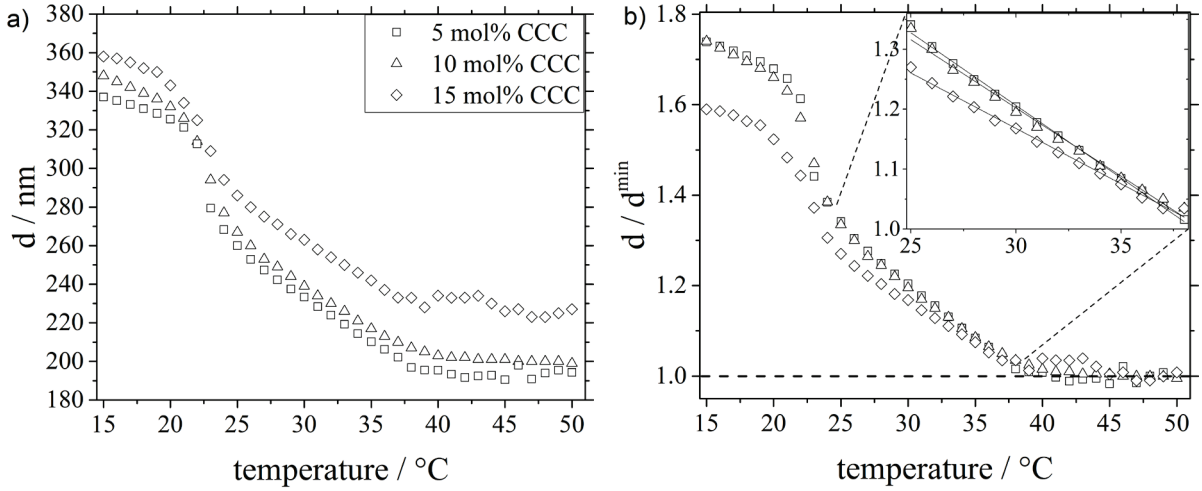

Figure 4: Ellipsometric measurements in water of the **a)** layer thickness d of core-shell microgels deposited on a silicon wafer, for different core crosslinker contents as indicated in the legend, as a function of temperature. In **b)**,

the curves are normalized to the high temperature average (45-50 °C) d^{min}, allowing a comparison of the swelling properties. The data clearly reveal the linear change in thickness of these layers. The inset shows a zoom of the linear region with the respective linear fits.

The main result shown in Figure 4 is the similarity of the swelling behavior in the adsorbed state compared to results found in suspension. In the intermediate T-range from 25 °C to 37 °C the layer thickness changes linearly. The resulting slopes are again found to depend on the CCC, and are reported in the inset of Figure 4b. They vary approximately by a factor 1.3, as the crosslinker content is increased from 5 to 15mol%. This agrees qualitatively with the results in suspension, where, however, a larger variation by a factor of 1.8 was found. The change in swelling is thus reduced, which might be due to a hindered swelling of particles due to van der Waals interactions with the surface.

In order to pursue the comparison between surface and bulk swelling properties in water, the corresponding normalized swelling curves obtained either by PCS (bulk) or ellipsometry (surface) are plotted for three different CCCs in Figure 5. As the curves are normalized to the high-temperature minimum hydrodynamic radius R_H^{min} and ellipsometric thickness d^{min}, respectively, they are naturally identical in the high-T range. In the intermediate-T range, where the linear swelling laws are observed, they superimpose almost equally well for all CCC. Again the above discussed lower change in slope of the adsorbed particles (Ellipsometry) compared to the particles in suspension (PCS) is observed, resulting in a small change from Fig 5a to 5c of the slope of the particles in suspension with respect to slope of the adsorbed ones. The evolution of the slopes with CCC has already been discussed with Figure 1 for bulk microgel particles: higher CCC leads to lower swelling. At the lowest temperatures, finally, the flattening and hindrance due to adsorption leads to the abovementioned reduced size of deposited microgels with respect to the freely suspended ones. Altogether, Figure 5 provides convincing evidence that free microgel particles in suspension and those adsorbed on wafers present the same linear swelling behavior, independently of the crosslinker content of the core.

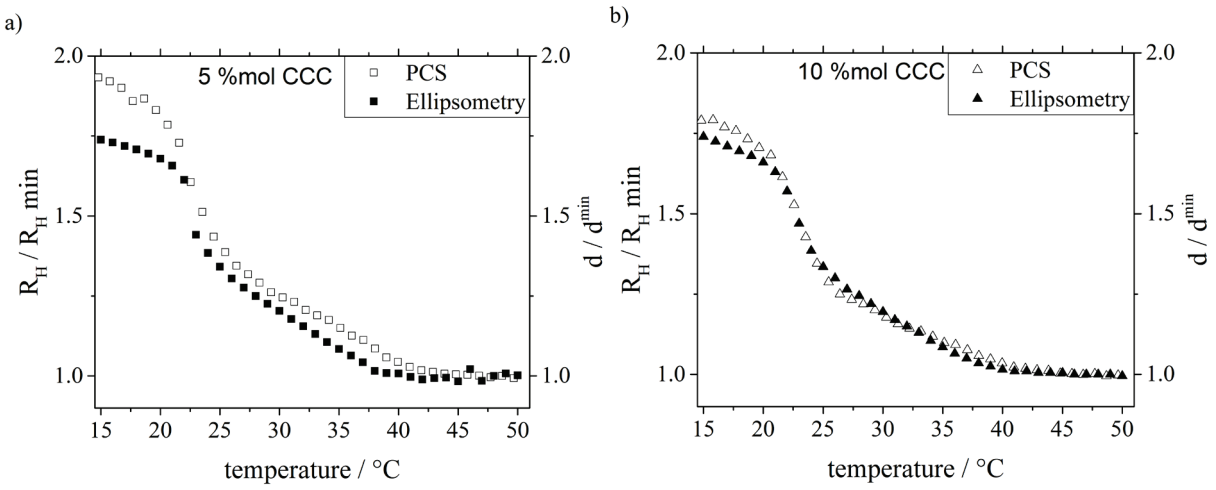

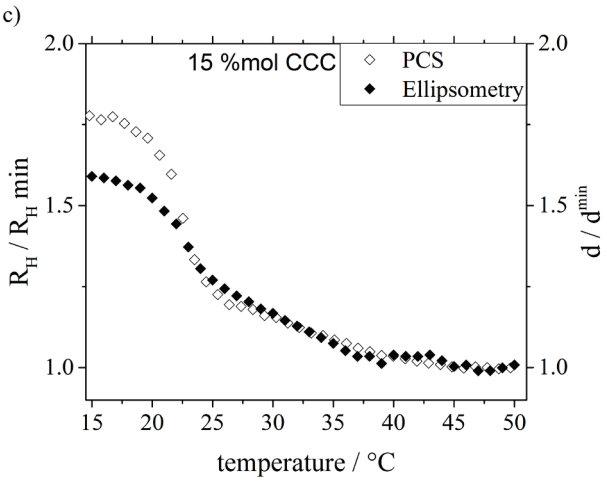

Figure 5: Swelling curves of hydrodynamic radius R_H or ellipsometric thickness d normalized to their high-temperature average (45 °C – 50 °C) of core-shell microgel particles in bulk (PCS, R_H/R_H^{min}) and on surfaces (ellipsometry, d/d^{min}), for different core crosslinker contents **a**) 5 mol% CCC **b**) 10 mol% CCC **c**) 15 mol% CCC).

Summary and Conclusion

In the present contribution, we have prepared surface coatings using core-shell microgels with core and shell made of two distinct polymers with a significant contrast in LCST (ΔLCST = 23 °C). The shell has the inferior LCST, thus it shrinks first as temperature is increased, and compresses the core. Inversely, starting from the high synthesis temperature and decreasing T, the core tends to swell first, but is hindered by the still collapsed shell, which leads to a peculiar – linear – swelling behavior. The slope of the evolution of the radius with temperature has been successfully correlated with the crosslinker density of the core: softer, less crosslinked cores have a stronger response. We have then deposited the microgel particles by spin-coating. The key result of this article is that the same particles respond also in a linear manner in size to temperature changes when they are adsorbed to a hard surface. In particular, we have shown by combinations of PCS, ellipsometry and AFM, that an extended linear behavior very similar to the one of the respective suspended particles persists, with a convincing overlap of the linear regions when expressed as relative swelling. Moreover, the average shape of individually adsorbed dry microgel particles has been measured by AFM. The total particle height could again be correlated with the core crosslinker density, the weaker microgels being flatter. The CCC is thus again shown to be the most important system parameter. Moreover, a volume analysis using the AFM height profiles allows an estimation of the average dry volume, and thus of the water content in suspension, in both the swollen and the collapsed state.

Such layers with a linear change in thickness might allow to tune, e. g., the interaction with vertebrate cells. Such a behavior might be of special interest in the context of stem cell differentiation since it can be expected that the Young modulus of the layers changes linearly and can be adjusted by the correct choice of the temperature. Moreover, such layers are certainly advantageous in microgel based etalons

[53,54]. As a promising perspective, one may explore the system where the LCST contrast is inverted. As the temperature is increased in such an inverse system, the core made of pNNPAM shrinks first (above 22°C), while the shell made of pNIPMAM is still in good solvent conditions. Such as system is expected to show completely different swelling curves, as well as modified mechanical properties.

Acknowledgements: The authors are thankful for support by the joint ANR/DFG CoreShellGel project, grant ANR-14-CE35-0008-01 of the French Agence Nationale de la Recherche, and grant HE2995/5-1 by Deutsche Forschungsgemeinschaft. We also thank Dagmar Wiechoczek for the help with the Karl-Fischer titration.

Supporting Information

PCS measurements of used PNIPMAM-cores, AFM images with different magnitudes and a sample for height profile extraction.

References

(1) Pelton, R. Temperature-sensitive aqueous microgels. *Adv. Colloid Interf. Sci.* **2000**, *85*, 1–33.

(2) Nayak, S.; Lyon, L. A. Soft Nanotechnology with Soft Nanoparticles. *Angew. Chem. Int. Ed.* **2005**, *44*, 7686–7708.

(3) Richtering, W.; Saunders, B. R. Gel architectures and their complexity. *Soft Matter* **2014**, *10*, 3695–3702.

(4) Ballauff, M.; Lu, Y. "Smart" nanoparticles: Preparation, characterization and applications. *Polymer* **2007**, *48*, 1815–1823.

(5) Dietsch, H.; Malik, V.; Reufer, M.; Dagallier; C.; Shalkevich, A.; Saric, M.; Gibaud, T.; Cardinaux, F.; Scheffold, F.; Stradner, A.; Schurtenberger, P. Soft Nanotechnology – from Colloid Physics to Nanostructured Functional Materials. *Chimia* **2008**, *62*, 805–814.

(6) Saunders, B. R.; Vincent, R. Microgel particles as model colloids: theory, properties, and applications. *Adv. Colloid Interf. Sci.* **1999**, *80*, 1–25.

(7) Geisel, K.; Henzler, K.; Guttmann, P.; Richtering, W. New Insight into Microgel-Stabilized Emulsions Using Transmission X-ray Microscopy: Nonuniform Deformation and Arrangement of Microgels at Liquid Interfaces. *Lamgmuir* **2015**, *31*, 83–89.

(8) Murray, M. J.; Snowden; M.J. The preparation, characterisation and applications of colloidal microgels. *Adv. Collloid Interf. Sci.* **1995**, *54*, 73–91.

(9) Berndt, I.; Pedersen, J. S.; Richtering, W. Temperature-Sensitive Core-Shell Microgel Particles with Dense Shell. *Angew. Chem.* **2006**, *118*, 1769–1773.

(10) Balaceanu, A.; Demco, D. E.; Möller, M.; Pich, A. Heterogeneous Morphology of Random Copolymer Microgels as Reflected in Temperature induced Volume Transition and ^{1}H High-Resolution Transverse Relaxation NMR. *Macromol. Chem. Phys.* **2011**, *212*, 2467–2477.

(11) Wedel, B.; Zeiser, M.; Hellweg, T. Non NIPAM Based Smart Microgels: Systematic Variation of the Volume Phase Transition Temperature by Copolymerization. *Zeitschrift f. Phys. Chem.* **2012**, *227*, 0–12.

(12) Wedel, B.; Brändel, T.; Bookhold, J.; Hellweg, T. Role of Anionic Surfactants in the Synthesis of Smart Microgels Based on Different Acrylamides. *ACS Omega* **2017**, *2*, 84–90.

(13) Wedel, B.; Hertle, Y.; Wrede, O.; Bookhold, J.; Hellweg, T. Smart Homopolymer Microgels: Influence of the Monomer Structure on the Particle Properties. *Polymers* **2016**, *8*.

(14) Yaodong Wu; Susanne Wiese; Andreea Balaceanu; Walter Richtering; Andrij Pich. Behavior of Temperature-Responsive Copolymer Microgels at the Oil/Water Interface. *Langmuir* **2014**, *30*, 7660–7669.

(15) Hoare, T.; Pelton, R. Dimensionless plot analysis: A new way to analyze functionalized microgels. *J. Coll. Interface. Sci.* **2006**, *303*, 109–116.

(16) Lally, S.; Bird, R.; Freemont, T. J.; Saunders, B. R. Microgels containing methacrylic acid: effects of composition on pH-triggered swelling and gelation behaviours. *Colloid Polym. Sci.* **2009**, *287*, 335–343.

(17) Kim, J.-H.; Ballauff, M. The volume transition in thermosensitive core-shell latex particles containing charged groups. *Colloid Polym. Sci.* **1999**, *277*, 1210–1214.

(18) Keerl, M.; Pedersen, J. S.; Richtering, W. Temperature Sensitive Copolymer Microgels with Nanophase Separated Structure. *J. Am. Chem. Soc.* **2009**, *131*, 3093–3097.

(19) Snowden, M. J.; Chowdhry, B. Z.; Vincent, B.; Morris, G. E. Colloidal copolymer microgels of N-isopropylacrylamide and acrylic acid: pH, ionic strength and temperature effects. *J. Chem. Soc., Faraday Trans.* **1996**, *92*, 5013–5016.

(20) Hertle, Y.; Hellweg, T. Thermoresponsive copolymer microgels. *J. Mater. Chem. B* **2013**, *1*, 5874–5885.

(21) Berndt, I.; Richtering, W. Doubly Temperature Sensitive Core-Shell Microgels. *Macromolecules* **2003**, *36*, 8780–8785.
(22) Lu, Y.; Mei, Y.; Drechsler, M.; Ballauff, M. Thermoresponsive Core-Shell Particles as Carriers for Ag Nanoparticles: Modulating the Catalytic Activity by a Phase Transition in Networks. *Angew. Chem. Int. Ed.* **2006**, *45*, 813–816.
(23) Duracher, D.; Elaissari, A.; Mallet, F.; Pichot, C. Adsorption of Modified HIV-1 Capsid p24 Protien onto Thermosensitive and Cationic Core-Shell Poly(styrene)-Poly(N-isopropylacrylamaide) Particles. *Langmuir* **2000**, *16*, 9002–9008.
(24) Hatto, N.; Cosgrove, T.; Snowden, M. J. Novel microgel-particle colloids: the detailed characterisation of the layer structure and chain topology of silica:poly(NIPAM) core-shell particles. *Polymer* **2000**, *41*, 7133–7137.
(25) Hellweg, T. Responsive Core-Shell Microgels: Synthesis, Characterization, and possible Applications. *J. Polymer Science Part B: Polymer Physics* **2013**, *51*, 1073–1083.
(26) Zeiser, M.; Freudensprung, I.; Hellweg, T. Linearly thermoresponsive core-shell microgels: Towards a new class of nanoactuators. *Polymer* **2012**, *53*, 6096–6101.
(27) Dubbert, J.; Honold, T.; Pedersen, J. S.; Radulescu, A.; Drechsler, M.; Karg, M.; Richtering, W. How Hollow Are Thermoresponsive Hollow Nanogels? *Macromolecules* **2014**, *47*, 8700–8708.
(28) Dubbert, J.; Nothdurft, K.; Karg, M.; Richtering, W. Core-shell-shell and hollow double-shell microgels with advanced temperature responsiveness. *Macromolecular rapid communications* **2015**, *36*, 159–164.
(29) Karg, M.; Wellert, S.; Prevost, S.; Schweins, R.; Dewhurst, C.; Liz-Marzán, L. M.; Hellweg, T. Well defined hybrid PNIPAM core-shell microgels: Size variation of the silica nanoparticle core. *Colloid Polym Sci* **2011**, *289*, 699–709.
(30) Königer, A.; Plack, N.; Köhler, W.; Siebenbürger, M.; Ballauff, M. Thermophoresis of thermoresponsive polystyrene–poly(N-isopropylacrylamide) core–shell particles. *Soft Matter* **2013**, *9*, 1418–1421.
(31) Schmidt, S.; Motschmann, H.; Hellweg, T.; Klitzing, R. von. Thermoresponsive surfaces by spin-coating of PNIPAM-co-PAA microgels. A combined AFM and ellipsometry study. *Polymer* **2008**, *49*, 749–756.
(32) Spears, M. W., JR; Herman, E. S.; Gaulding, J. C.; Lyon, L. A. Dynamic materials from microgel multilayers. *Langmuir the ACS journal of surfaces and colloids* **2014**, *30*, 6314–6323.
(33) Vikulina, A. S.; Aleed, S. T.; Paulraj, T.; Vladimirov, Y. A.; Duschl, C.; Klitzing, R. von; Volodkin, D. Temperature-induced molecular transport through polymer multilayers coated with PNIPAM microgels. *Physical chemistry chemical physics PCCP* **2015**, *17*, 12771–12777.
(34) Islam, M. R.; Serpe, M. J. Poly (N -isopropylacrylamide) microgel-based etalons and etalon arrays for determining the molecular weight of polymers in solution. *APL Materials* **2013**, *1*, 52108.
(35) Nerapusri, V.; Keddie, J. L.; Vincent, B.; Bushnak, I. A. Absorption of cetylpyridinium chloride into poly(N-isopropylacrylamide)-based microgel particles, in dispersion and as surface-deposited monolayers. *Langmuir the ACS journal of surfaces and colloids* **2007**, *23*, 9572–9577.
(36) Howard, S. C.; Craig, V. S. J.; FitzGerald, P. A.; Wanless, E. J. Swelling and collapse of an adsorbed pH-responsive film-forming microgel measured by optical reflectometry and QCM. *Langmuir the ACS journal of surfaces and colloids* **2010**, *26*, 14615–14623.
(37) Höfl, S.; Zitzler, L.; Hellweg, T.; Herminghaus, S.; Mugele, F. Volume phase transition of “smart” microgels in bulk solution and adsorbed at an interface: A combined AFM, dynamic light, and small angle neutron scattering study. *Polymer* **2007**, *48*, 245–254.
(38) Herman, E. S.; Lyon, L. A. Polyelectrolyte exchange and diffusion in microgel multilayer thin films. *Colloid Polym Sci* **2015**, *293*, 1535–1544.

(39) Clarke, K. C.; Dunham, S. N.; Lyon, L. A. Core/Shell Microgels Decouple the pH and Temperature Responsivities of Microgel Films. *Chem. Mater.* **2015**, *27*, 1391–1396.
(40) Schmidt, S.; Zeiser, M.; Hellweg, T.; Duschl, C.; Fery, A.; Möhwald, H. Adhesion and Mechanical Properties of PNIPAM Microgel Films and Their Potential Use as Switchable Cell Culture Substrates. *Adv. Func. Mater.* **2010**, *20*, 3235–3243.
(41) Uhlig, K.; Wegener, T.; He, J.; Zeiser, M.; Bookhold, J.; Dewald, I.; Godino, N.; Jaeger, M.; Hellweg, T.; Fery, A.; Duschl, C. Patterned Thermoresponsive Microgel Coatings for Noninvasive Processing of Adherent Cells. *Biomacromolecules* **2016**, *17*, 1110–1116.
(42) Smiley-Wiens, J. B.; Serpe, M. J. Solvent exchange kinetics in poly(N-isopropylacrylamide) microgel-based etalons. *Colloid Polym Sci* **2013**, *291*, 971–979.
(43) Sorrell, C. D.; Serpe, M. J. Glucose sensitive poly (N-isopropylacrylamide) microgel based etalons. *Analytical and bioanalytical chemistry* **2012**, *402*, 2385–2393.
(44) Hirano, T.; Nakamura, K.; Kamikubo, T.; Ishii, S.; Tani, K.; Mori, T.; Sato, T. Hydrogen-bond-assisted syndiotactic-specific radical polymerizations ofN-alkylacrylamides: The effect of theN-substituents on the stereospecificities and unusual large hysteresis in the phase-transition behavior of aqueous solution of syndiotactic poly(N-n-propylacrylamide). *Journal of Polymer Science Part A: Polymer Chemistry* **2008**, *46*, 4575–4583.
(45) Provencher, S. W. A constrained regularization method for inverting data represented by linear algebraic or integral equations. *Computer Physics Com* **1982**, *27*, 213–217.
(46) Provencher, S. W. Contin: a general purpose constrained regularization program for inverting noisy linear algebraic and integral equations. *Computer Physics Com* **1982**, *27*, 229–242.
(47) Bonn, D.; Wegdam, G. H.; Kellay, H.; Nieuwenhuizen, T. M. Molecular Layering on a Fluid Substrate. *Europhys. Lett.* **1992**, *20*, 235–239.
(48) Beaglehole, D. Ellipsometric Study of the Surface of Simple Liquids. *Physica B* **1980**, *100*, 163–174.
(49) Nerapusri, V.; Keddie, J. L.; Vincent, B.; Bushnak, I. A. Swelling and Deswelling of Adsorbed Microgel Monolayers Triggered by Changes in Temperature, pH, and Electrolyte Concentartion. *Langmuir* **2006**, *22*, 5036–5041.
(50) Nečas, D.; Klapetek, P. Gwyddion: an open-source software for SPM data analysis. *Open Physics* **2012**, *10*.
(51) Gawlitza, K.; Georgieva, R.; Tavraz, N.; Keller, J.; Klitzing, R. von. Immobilization of water-soluble HRP within poly-N-isopropylacrylamide microgel particles for use in organic media. *Langmuir the ACS journal of surfaces and colloids* **2013**, *29*, 16002–16009.
(52) Tompkins H. G. *A User's Guide to Ellipsometry*; Dover Publications: Newburyport, 2013.
(53) Zhang, Q. M.; Berg, D.; Mugo, S. M.; Serpe, M. J. Lipase-modified pH-responsive microgel-based optical device for triglyceride sensing. *Chem. Commun.* **2015**, *51*, 9726–9728.
(54) Sorrell, C. D.; Carter, M. C. D.; Serpe, M. J. Color Tunable Poly(N-Isopropylacrylamide)-co-Acrylic Acid Microgel-Au Hybrid Assemblies. *Adv. Func. Mater.* **2011**, *21*, 425–433.

For Table of Contents Only: